DIAMOND LIGHT SOURCE BOOSTER FAST ORBIT FEEDBACK SYSTEM

S. Gayadeen, S.R. Duncan, University of Oxford, Oxfordshire, UK,
C. Christou, M.T. Heron, J. Rowland, Diamond Light Source, Oxfordshire,UK

Abstract

The Fast Orbit Feedback system that has been installed on the Diamond Light Source Storage ring has been replicated on the Booster synchrotron in order to provide a test bed for the development of the Storage Ring controller design. To realise this the Booster is operated in DC mode. The electron beam is regulated in two planes using the Fast Orbit Feedback system, which takes the beam position from 22 beam position monitors for each plane, and calculates offsets to 44 corrector power supplies at a sample rate of 10 kHz. This paper describes the design and realization of the controller for the Booster Fast Orbit Feedback, presents results from the implementation and considers future development.

INTRODUCTION

The Diamond Storage Ring Fast Orbit Feedback (FOFB) system currently meets its requirements in terms of beam stability at Diamond. However new requirements for improved beam stability, from users or as a consequence of operating with reduced electron beam height or a need to suppress new beam disturbances in the future, will require improvements to the FOFB performance. As part of the development of the Storage Ring controller optimisation, closed loop beam control has been applied on the Booster synchrotron by running the Booster as an electron storage ring at 100 MeV. The Booster has the same hardware as the Storage Ring for beam position detection and control of the corrector magnets, so the same FOFB control system can be used.

CONTROLLER DESIGN

Let $\mathbf{P}(z^{-1})$ denote the discrete-time transfer function between $\mathbf{u}[k] \in \mathbb{R}^N$, the inputs to the $N = 22$ actuators applied at time $\{t = kT\}$, where T is the sample time, and $\mathbf{y}[k] \in \mathbb{R}^M$, the signals measured at the $M = 22$ sensors at each sample time, such that

$$\mathbf{y}[k] = \mathbf{P}(z^{-1})\mathbf{u}[k] \tag{1}$$

where $\mathbf{P}(z^{-1})$ takes the form

$$\mathbf{P}(z^{-1}) = p(z^{-1})\mathbf{B} \tag{2}$$

with $\mathbf{B} \in \mathbb{R}^{M\times N}$ being the steady state (dc) response of the actuators and $p(z^{-1})$ the scalar dynamics, which are taken to be the same for each actuator. The dynamics are modeled as a first order response plus delay that is operated in "sample and hold" mode, then

$$p(z^{-1}) = z^{-d}\frac{b_0 + b_1 z^{-1}}{1 - a_1 z^{-1}} \tag{3}$$

where d is the smallest integer satisfying $dT > \tau_d$ and

$$\begin{aligned} a_1 &= e^{-aT} \\ b_0 &= 1 - e^{a(T-\tau')} \\ b_1 &= e^{a(T-\tau')} - e^{-aT} \end{aligned} \tag{4}$$

when τ_d is the delay in the system, a is the bandwidth of the actuator response (in rad.s^{-1}) and

$$\tau' = \tau_d - (d-1)T. \tag{5}$$

Table 1: Values of Parameters Used in Design

Parameter	Value
a	$2\pi\times1000$ rad.s^{-1}
τ_d	700 μs
T	100 μs

The parameters associated with this application are listed in Table so that the transfer function for the dynamic response becomes

$$p(z^{-1}) = z^{-7}\frac{0.47z^{-1}}{1 - 0.53z^{-1}}. \tag{6}$$

For $M \leq N$, the singular value decomposition of $\mathbf{B}$ takes the form

$$\mathbf{B} = \mathbf{U}\,[\Sigma\ \ 0]\,\mathbf{V}^T \tag{7}$$

where $\mathbf{U} \in \mathbb{R}^{M\times M}$ and $\mathbf{V} \in \mathbb{R}^{N\times N}$ are respectively, the left and right singular vectors and $\Sigma \in \mathbb{R}^{M\times M}$ is a diagonal matrix containing the singular values, $\sigma_1 \geq \sigma_2 \geq \ldots \geq \sigma_M$. By partitioning $\mathbf{V}$ as

$$\mathbf{V} = [\mathbf{V}_1\ \mathbf{V}_2] \tag{8}$$

where $\mathbf{V}_1 \in \mathbb{R}^{N\times M}$ and $\mathbf{V}_2 \in \mathbb{R}^{N\times(N-M)}$, so that $\mathbf{B} = \mathbf{U}\Sigma\mathbf{V}_1^T$, then Eq. (1) can be written as

$$\mathbf{U}^T\mathbf{y}[k] = p(z^{-1})\Sigma{\mathbf{V}_1}^T\mathbf{u}[k]. \tag{9}$$

Defining $\bar{\mathbf{y}}[k] = \mathbf{U}^T\mathbf{y}[k]$ and $\bar{\mathbf{u}}[k] = \mathbf{V}_1^T\mathbf{u}[k]$, projects the response into "modal space", so that

$$\bar{y}_n[k] = p(z^{-1})\bar{u}_n[k] \tag{10}$$

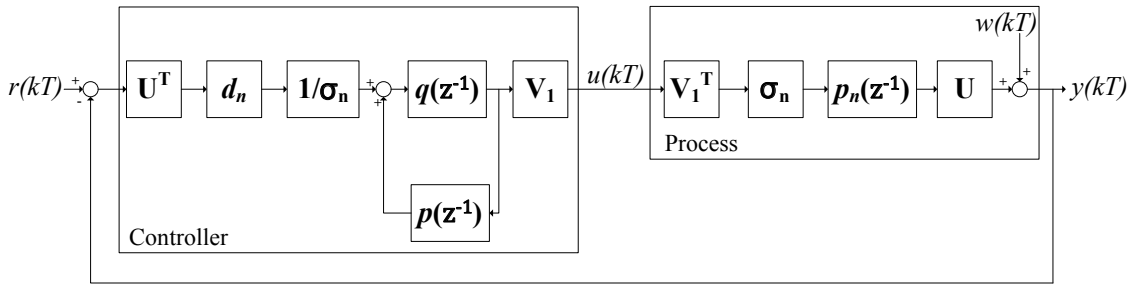

Figure 1: Structure of IMC controller.

where $\bar{y}_n[k]$ and $\bar{u}_n[k]$ are the n^{th} elements of $\bar{\mathbf{y}}[k]$ and $\bar{\mathbf{u}}[k]$. The controller structure is shown in Fig. 1 where an Internal Model Controller (IMC) [1] is applied to each mode where $q(z^{-1})$, the pseudo plant inverse dynamics is given by

$$q(z^{-1}) = \frac{(1-\lambda)}{b_o + b_1}\frac{1 - a_1 z^{-1}}{1 - \lambda z^{-1}} \tag{11}$$

and $\lambda = e^{-\zeta T}$ where ζ is the closed loop bandwidth (in rad.s^{-1}) of the controller. In [2, 3] it is proposed that the controller should take the form

$$\mathbf{C}(z^{-1}) = c(z^{-1})\mathbf{C} \tag{12}$$

where $\mathbf{C} \in \mathbb{R}^{N\times M}$ is

$$\mathbf{C} = \mathbf{V_1}\mathbf{D}\Sigma^{-1}\mathbf{U}^T \tag{13}$$

where

$$\begin{aligned}\mathbf{D} &= \text{diag}\{d_n\}\\ \Sigma &= \text{diag}\{\sigma_n\}\end{aligned} \tag{14}$$

with

$$d_n = \frac{\sigma_n^2}{\sigma_n^2 + \mu} \tag{15}$$

From Fig. 1 the controller dynamics for each mode are

$$\begin{aligned}c(z^{-1}) &= \frac{q(z^{-1})}{1 - p(z^{-1})q(z^{-1})}\\ &= \frac{(1-\lambda)}{b_0 + b_1}\frac{1 - a_1 z^{-1}}{1 - \lambda z^{-1} - z^{-d}(1-\lambda)\beta(z^{-1})}\end{aligned} \tag{16}$$

with

$$\beta(z^{-1}) = \beta_0 + \beta_1 z^{-1} = \frac{b_0 + b_1 z^{-1}}{(b_0 + b_1)}. \tag{17}$$

The same controller dynamics are applied to each spatial mode, with the dynamics being detuned by the controller gains d_n. Because $\beta_0 + \beta_1 = 1$, the controller takes the form of a Dahlin controller [4] and as a result, includes integral action.

CONTROLLER IMPLEMENTATION

Electron BPMs are used to provide information about the electron beam position at a sampling rate of 10 kHz. The Booster has 22 cells arranged as 4 sectors each of which has a computation node which receives all sensor positions but only calculates the local corrector magnet error using a block of the inverse response matrix. To achieve the required 10 kHz update rate, a custom communication controller implemented in VHDL is used to transmit the horizontal and vertical data from the 22 BPMs to each of the 4 computation nodes. Each computation node receives data from all BPMs and uses a dedicated VME processor card to calculate the vector product of the BPM values and the sub pseudo-inverse response matrix. The controller dynamics are then implemented as an eighth order IIR filter on these values. The result then corresponds to the new values for the local corrector magnets for that sector [5].

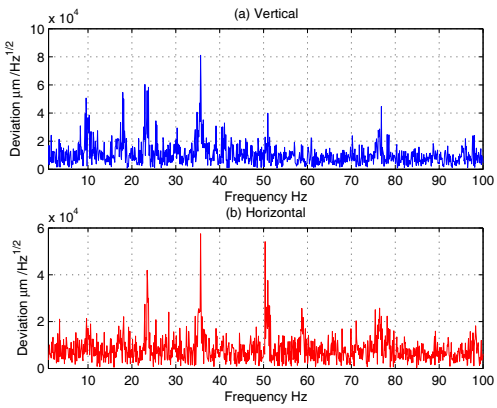

Figure 2: Magnitude of frequency response of 10s of variation observed at the 1st vertical BPM plotted against frequency in Hz.

CONTROLLER PERFORMANCE

The frequency content of the disturbance at one BPM on the Booster is shown in Fig. 2, which plots the discrete Fourier transform of the signal against frequency. It can be seen that there is a significant component in the range 10 Hz to 50 Hz with a major peak at 35 Hz. Fig 3(a) shows a colourmap of the average power (in dB) at each frequency in mode space and it can be seen that the bulk of the power is concentrated in the lower order modes (i.e. for n <10).

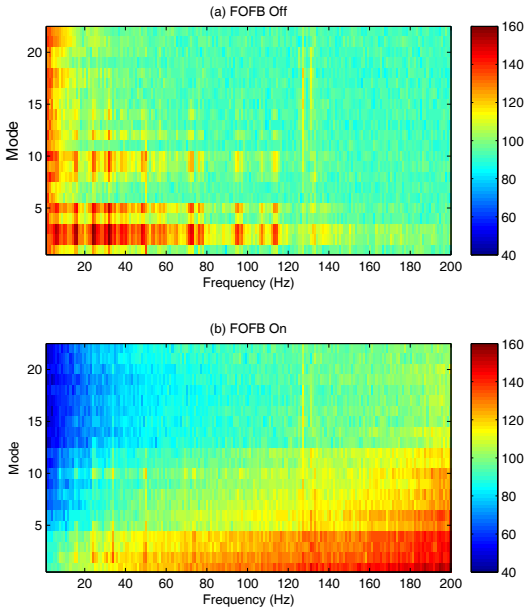

Figure 3: Colourmap of average power (in dB) in mode space against frequency (in Hz) in the vertical plane with (a) FOFB off and (b) FOFB on.

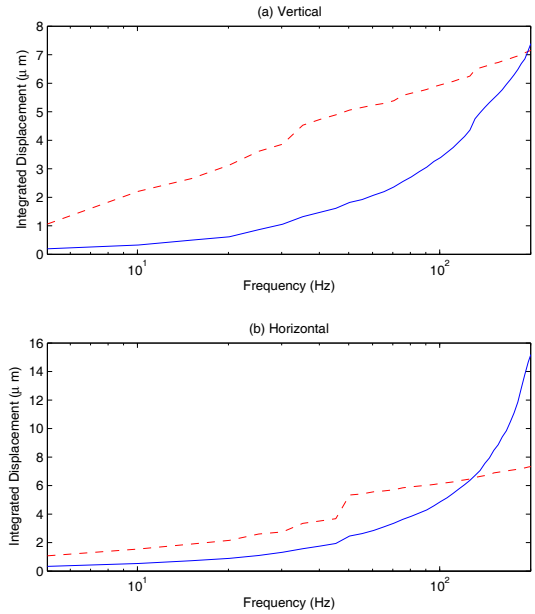

Figure 4: Integrated beam motion for controlled (solid blue line) and uncontrolled (dashed red line) beam up to 200 Hz.

There is also some variation at low frequencies (<1 Hz) in all modes.

The aim of the control system is to reduce the effect of the disturbances on the beam, particularly for the low order modes in the frequency range 10 Hz to 50 Hz, while at the same time attenuating low frequency disturbances in all modes. Figure 3(b) shows the power spectrum with FOFB on and by comparison with Fig. 3(a), it can be seen that the attenuation is focused on the low frequencies for all modes (i.e. the dark blue regions). The controlled and uncontrolled integrated beam motion for both planes, shown in Fig. 4, illustrates that the FOFB suppresses beam motion in the low frequencies where the disturbances are concentrated. However the FOFB system does not suppress disturbances as well at frequencies above to 200 Hz in both planes.

TWO DIMENSIONAL LOOP SHAPING

When a disturbance $\mathbf{w}[k]$ is included in the output $\mathbf{y}[k]$, then by defining $\overline{\mathbf{w}}[k] = \mathbf{U}_1^T \mathbf{w}[k]$, for each mode, $s_n(z^{-1})$, the transfer function from $\overline{\mathbf{w}}[k]$ to the output, $\overline{\mathbf{y}}[k]$ i.e. the sensitivity function is

$$s_n(z^{-1}) = \frac{1 - \lambda z^{-1} - z^{-d}(1-\lambda)(\beta_0 + \beta_1 z^{-1})}{1 - \lambda z^{-1} - z^{-d}(1-d_n)(1-\lambda)(\beta_0 + \beta_1 z^{-1})}$$

which can be used to analyse the behaviour of the closed loop system in Fig. 1. Figure 5 shows the Booster sensitivity both spatial and temporal dimensions $S(n, e^{-j2\pi\omega})$. The plane in Fig. 5 shows where $|S(n, e^{-j2\pi\omega})| = 0.7071$ i.e. the crossover frequency in both dimensions.

The bandwidth in the two-dimensional frequency domain can be similarly defined as traditionally done in the temporal frequency domain so that the closed loop bandwidth $\mathbf{B}_w(n,\omega)$ is defined as the contour in (n,ω) such that $|S(n, e^{j2\pi\omega})| = \frac{1}{\sqrt{2}}$ for all (n,ω) enclosed by $\mathbf{B}_w(n,\omega)$ [6]. The two-dimensional bandwidth frequency bandwidth contour is shown in Fig. 6 which also shows the effect of changing the regularisation parameter, μ and the closed-loop bandwidth, ζ. Figure 6(a) illustrates that increasing μ, focuses control effort on the lower order modes and decreasing μ, extends control to the higher order modes. It can also be seen that although μ has a significant impact on the spatial bandwidth, in this case it has no effect on the temporal component of the two-dimensional bandwidth $\mathbf{B}_w(n,\omega)$. Figure 6(b) illustrates that decreasing ζ, reduces the bandwidth to attenuate disturbances and has a negligible effect on the spatial component of the bandwidth $\mathbf{B}_w(n,\omega)$. From Fig. 6(b) it can be said that decreasing ζ has the effect of depressing the peak of the sensitivity function while reducing its temporal bandwidth.

The expected value of total power in the output is

$$E\|\mathbf{y}[k]\|_2^2 = \frac{1}{K}\sum_{k=0}^{K-1}\|\mathbf{y}[k]\|_2^2 \qquad (18)$$

In [2], it is shown that the expected total power can be written as

$$E\|\bar{\mathbf{y}}[k]\|_2^2 = \frac{1}{K^2}\sum_{p=0}^{K-1}\sum_{n=1}^{N}|S_n[p]|^2|\bar{W}_n[p]|^2 \qquad (19)$$

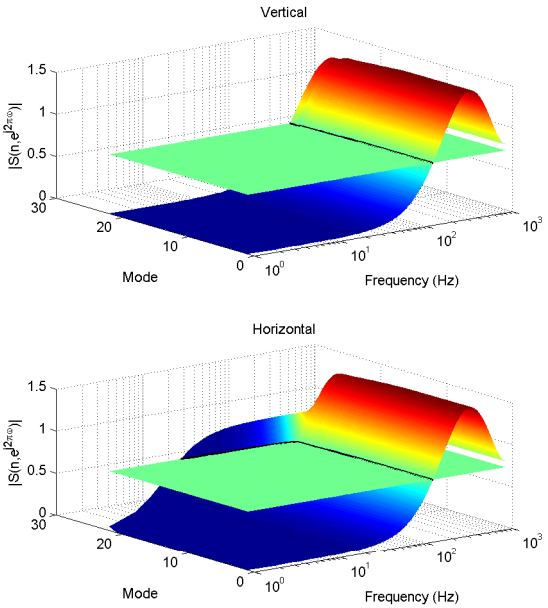

Figure 5: Magnitude of sensitivity ($|S(n, e^{i2\pi\omega})|$)for each mode against frequency (in Hz). The plane for $|S(n, e^{j2\pi\omega})| = 0.7071$ and the two-dimensional bandwidth contour (black line) are shown.

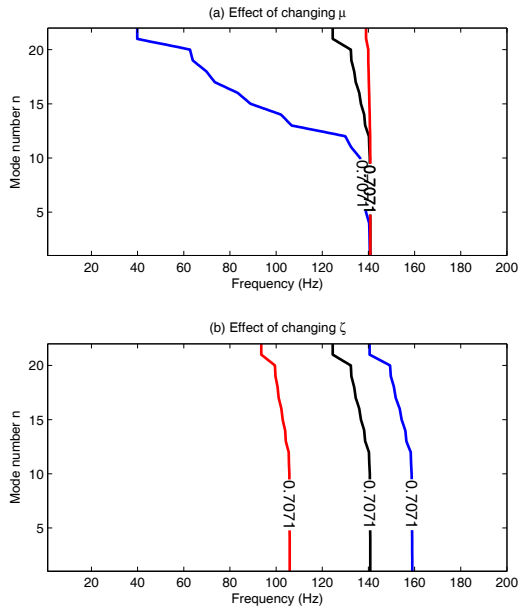

Figure 6: Two-dimensional bandwidth for (a) μ =0.1 (red), μ =1 (black) and μ =20 (blue) (b) ζ =303 Hz (red), ζ =227 Hz (black) and ζ =129 Hz (blue).

where $S_n[p]$ is the frequency response of $s_n(z^{-1})$. Eq. (19) implies that given $\bar{W}_n[p]$, the frequency spectrum of each mode of the underlying disturbance, $S_n[p]$ (and hence $s_n(z^{-1})$) can be designed on a "mode-by-mode" basis in order to achieve a specification on the expected total power observed across all sensors.

CONCLUSIONS & FUTURE WORK

FOFB control has been implemented on the Booster synchrotron at Diamond. The controller has been tuned conservatively and initial results show that the controller attenuates disturbances below 100 Hz on all modes.

The loop shaping technique developed by [6] shows that by extending traditional loop shaping techniques for dynamical systems into the two dimensional frequency domain, a framework to analyse the properties of the sensitivity function in the two-dimensional frequency domain analysis can be constructed. The sensitivity function properties in both temporal and spatial modes are used to define a two-dimensional bandwidth.

It was illustrated that tuning the temporal and spatial components of the sensitivity can be decoupled by using the dynamic closed loop bandwidth, ζ for shaping the temporal frequency response and the regularisation parameter, μ for the spatial frequency response. By considering the residual power in the output, it was demonstrated that given the frequency spectrum of each mode of the underlying disturbance, the sensitivity function can be designed on a mode-by-mode basis in order to achieve a specification on the expected average power across all sensors.

REFERENCES

[1] M. Morari and E. Zafiriou. *Robust Process Control*. Prentice Hall, 1989.

[2] S.R. Duncan. The design of a fast orbit beam stabilisation system for the diamond synchrotron. Technical Report 2296/07, University of Oxford, 2007.

[3] A. Napier, S. Gayadeen, and S.R. Duncan. Fast orbit beam stabilisation for a synchrotron. In *IEEE Multi-Conference on Systems and Control*, Denver, CO, 2011.

[4] D. Seborg, T. Edgar, D. Mellichamp, and F. Doyle III. *Process Dynamics and Control*. John Wiley and Sons, 2011.

[5] J. Rowland, M.G. Abbott, R. Bartolini, J.A. Dobbing, M.T. Heron, I. Martin, G. Rehm, I. Uzun, and S.R. Duncan. Status of the diamond fast orbit feedback system. In *Proc. Int. Conf. on Accelerator and LArge Experimental Physics Control Systems*, Knoxville, TN, 2007.

[6] G.E. Stewart. Two-dimensional loop shaping. *Automatica*, 39:779–792, 2003.